J. Cent. South Univ. (2017) 24: 48−55
DOI: 10.1007/s11771-017-3407-y

Springer

Liquidus and phase equilibria in $CaO-SiO_2-5\%MgO-20\%Al_2O_3-TiO_2$ system

SUN Li-feng(孙丽枫)[1, 2], SHI Jun-jie(石俊杰)[1, 2], ZHANG Bo(张波)[1, 2], QIU Ji-yu(邱吉雨)[1, 2], WANG Zhao-yun(王昭云)[1, 2], JIANG Mao-fa(姜茂发)[1, 2]

1. School of Metallurgy, Northeastern University, Shenyang 110819, China;
2. Key Laboratory for Ecological Metallurgy of Multimetallic Ores of Ministry of Education (Northeastern University), Shenyang 110819, China

Abstract: The single hot thermocouple technique (SHTT) and high temperature equilibrium technique were combined to investigate the phase diagram of the $CaO-SiO_2-5\%MgO-20\%Al_2O_3-TiO_2$ system. The 1300 °C to 1500 °C liquidus lines are calculated according to the thermodynamic equations based on the pseudo-melting temperatures measured by the single hot thermocouple technique. The phase equilibria relationships are experimentally determined at 1400 °C using the high temperature equilibria technique followed by X-ray fluorescence (XRF), X-ray diffraction(XRD), scanning electron microscopy (SEM) and energy dispersive X-ray spectroscopy (EDX) analysis. The liquid phase(*L*), melilite solid solution phase ($(C_2MS_2,C_2AS)_{ss}$), diopside phase(CMS_2) and perovskite phase ($CaO{\cdot}TiO_2$) are found. Coupled with the liquidus lines and equilibria results, the phase diagram is constructed for the specified region of the $CaO-SiO_2-5\%MgO-20\%Al_2O_3-TiO_2$ system.

Key words: phase diagram; liquidus; equilibrium; TiO_2; single hot thermocouple technique (SHTT); thermodynamics

1 Introduction

Titanium-bearing blast furnace slag (Ti-bearing slag) produced by the iron and steel industry, which contains more than 20% TiO_2 [1], has been considered valuable secondary resource. A number of methods have been developed to study the properties of Ti-bearing slag, such as the acid leading [2, 3], carbide−chloride method [4−6] and the selective crystallization and phase separation method [7, 8]. The liquidus temperatures and phase relations of Ti-bearing slag are necessary to facilitate improvements to the related processes. However, the phase diagrams were difficult to study due to the complex reactions among the components.

The phase diagrams of Ti-bearing slag system were only studied by a few authors [9−12]. OLLNO et al [9] measured the liquidus temperatures and primary phases in a wide TiO_2 range for $CaO-SiO_2-TiO_2-Al_2O_3$ systems with 10% and 20% Al_2O_3 using the hot stage thermocouple in air atmosphere. OSBORN et al [10] studied the effect of TiO_2 addition on liquidus temperatures of $CaO-SiO_2-MgO-Al_2O_3$ system in air atmosphere and the results indicated that the liquidus temperatures were not greatly influenced. The phase equilibrium at reducing condition was studied by ZHAO et al [11] and the new phases of perovskite and anosovite were formed with the addition of TiO_2 to $CaO-SiO_2-MgO-Al_2O_3$ system. However, the comprehensive phase relations of the $CaO-SiO_2-MgO-Al_2O_3-TiO_2$ system still remain unclear and the lack of thermodynamic information for liquidus temperatures and phase relations seriously retards the development and application of above mentioned system.

The traditional way of phase diagrams investigation is the high-temperature equilibrium and quenching method, which exhausts a large amount of time. In the present work, a method of the combination of the single hot thermocouple technique (SHTT) and high-temperature equilibrium technique was used to construct the phase diagram of Ti-bearing slag system, which has been proven as an accurate, reproducible and reliable method for determining the phase diagram of oxide system [13, 14]. Firstly, the pseudo-melting temperatures were measured by SHTT, which can achieve in situ observation of the melting process, and the liquidus temperatures could be calculated subsequently according to the thermodynamic equations.

Foundation item: Projects(51104039, 51374059, 51304042) supported by the National Natural Science Foundation of China; Project(L2013114) supported by Scientific Research Fund of Liaoning Provincial Education Department, China; Project(2012221013) supported by Programs of Liaoning Province for Science and Technology Development, China; Project(N130602002) supported by the Fundamental Research Funds for the Central Universities China
Received date: 2015−10−08; **Accepted date:** 2016−03−22
Corresponding author: SHI Jun-jie, Doctoral Candidate; Tel: +86−15840571858; E-mail: 1110221@stumail.neu.edu.cn

After the establishment of the liquidus lines, only a few number of equilibria experiments were needed to confirm the primary phases of the different compositions. The method used in this work could save abundant time without reducing the measurement accuracy. The investigation described here was one part of a long-term study for Ti-bearing slag system and the results from the present study could provide important information for the optimization of the thermodynamic database.

2 Experimental

2.1 Sample preparation

Reagent grade oxides powders of CaO, SiO_2, MgO, Al_2O_3 and TiO_2 were employed to synthesize the slags, which were calcined at 1000 °C for 4 h to evaporate the moisture and impurities respectively and carefully weighed, fully mixed and pre-melted in Ar atmosphere using vertical $MoSi_2$ furnace. The mixtures were placed inside platinum crucibles which were suspended by platinum wire inside of hot zone of the furnace at 1650 °C for 2 h to completely homogenize the slags, after that, the liquid slags were rapidly poured into ice water to obtain the glassy slags. The XRD analyses proved that the quenched slags showed glassy phase. Subsequently, the glassy slags were dried, crushed and grounded under 45 μm for further utilization. The compositions of pre-melted slags were analyzed by X-ray fluoroscopy (XRF), as listed in Table 1.

Table 1 Compositions of pre-melted slags

No.	w(CaO)/w(SiO_2)	Mass fraction after pre-melting/%				
		CaO	SiO_2	MgO	Al_2O_3	TiO_2
M1	1.52	42.72	28.11	5.29	19.34	4.54
M2	1.45	40.61	28.00	6.12	20.62	4.65
M3	0.94	33.37	35.50	5.45	20.77	4.91
M4	1.31	40.43	30.87	5.04	18.45	5.21
M5	1.02	34.96	34.28	5.11	20.25	5.40
M6	0.90	30.65	34.06	5.20	20.96	9.13
M7	1.56	39.54	25.35	5.27	20.22	9.62
M8	1.03	34.01	33.01	4.84	18.29	9.85
M9	1.09	33.51	30.75	5.36	19.79	10.59
M10	1.45	38.52	26.56	5.25	19.37	10.30
M11	1.66	38.78	23.36	4.44	19.19	14.23
M12	1.45	36.64	25.27	5.01	18.11	14.97
M13	1.00	30.95	30.95	4.28	18.23	15.60
M14	1.58	35.78	22.64	4.58	18.35	18.65
M15	1.13	30.12	26.66	5.44	18.92	18.86
M16	0.90	26.66	29.63	5.53	19.22	18.96
M17	1.79	35.74	19.97	4.33	19.22	20.74
M18	1.21	27.28	22.54	4.12	19.06	27.00
M19	0.92	32.62	35.45	5.96	20.64	5.33
M20	1.10	36.29	33.00	5.90	19.80	5.01
M21	1.36	40.07	29.47	6.04	19.24	5.18
M22	1.60	43.15	26.97	5.91	19.00	4.97
M23	0.98	32.44	33.10	5.37	18.91	10.18
M24	1.15	35.20	30.61	5.63	18.89	9.67
M25	1.39	38.44	27.65	5.58	18.28	10.05
M26	1.64	41.31	25.19	5.06	18.86	9.58
M27	0.98	30.28	30.90	5.15	18.54	15.13
M28	1.21	33.61	27.77	5.07	18.24	15.31
M29	1.37	35.22	25.71	4.78	19.32	14.97
M30	1.71	38.52	22.53	4.98	19.54	14.43
M31	1.00	26.88	26.88	4.79	19.67	21.79
M32	1.25	30.23	24.19	4.92	19.85	20.81
M33	1.52	34.54	22.72	4.94	19.87	17.93
M34	1.76	36.16	20.54	5.19	19.93	18.18
M35	1.09	25.30	23.21	4.43	18.78	28.28
M36	1.26	28.38	22.53	4.79	18.66	25.64
M37	1.52	30.54	20.10	4.57	18.96	25.83
M38	1.76	33.57	19.07	5.17	19.62	22.57

2.2 Pseudo-melting temperature determination

The SHTT technique was employed to measure the pseudo-melting temperatures of the slags in the present experiments. The application of SHTT technique for temperature measuring has been proven as an effective method based on the previous work [9] and the results from the present authors [13, 14]. The principle of SHTT has been described in details [15−17] and is briefly summarized in this work. A B-type thermocouple (0.2−mm in diameter) was used to heat and measure the temperature simultaneously. A microscope equipped with a video camera was applied to in-situ observe and record the images of slag, which were sent to a computer and a video cassette recorder. The heating process was controlled by a computer program.

The following method, as illustrated in Fig. 1, was used for the judgements of the pseudo-melting temperatures. During the experiments, approximately 10 mg slag was mounted at the tip of thermocouple, since the temperature was most accurate at the tip of the thermocouple and the part of the slag surrounding the tip of the thermocouple was chosen for observing and measuring, as shown in the circular arc area in Fig. 1. The temperature was rapidly heated at 5−10 °C/s to 50−200 °C below the approximate melting temperature. It was clearly seen that the slag was completely solid at this temperature. Then, the slag was heated continuously with a very slow rate of 0.1 °C/s to the temperature

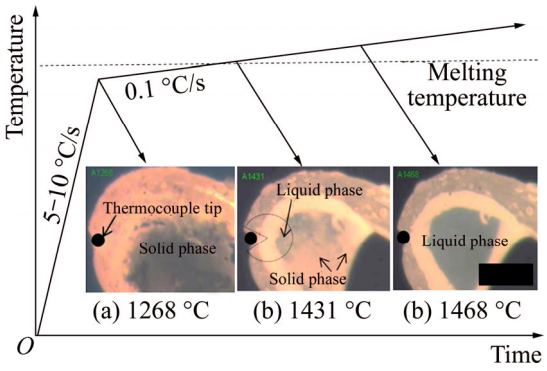

Fig. 1 Graphical representation for pseudo-melting temperature determination

shown in Fig. 1(b), at which the slag close to the tip of the thermocouple first became fluidity and transparent while the slag far away from the thermocouple tip was still solid phase, which meant that the slag around the thermocouple tip had already been liquid phase. The temperature of the state in Fig. 1(b) was found reproducible and taken as the melting temperature of the slag, which was called pseudo-melting temperature in this work. With the temperature future increased, the left slag gradually became liquid due to the heat transfer in Fig. 1(c). The whole melting process of the slag was recorded as a video file and the pseudo-melting temperature was then obtained.

Each measurement was performed at least three times to verify the reproducibility. The B-type thermocouple was calibrated against the pure NaF and CaF_2 to ensure the temperature accuracy within ±1 °C.

2.3 Equilibria experiments

The high-temperature equilibria technique [18] was employed to acquire the crystallization information for the slags. The vertical furnace used for pre-melting experiments was employed for the equilibria experiments. The furnace temperature was monitored by a B-type thermocouple placed next to the samples with an overall temperature accuracy estimated to be ±2 °C. The platinum crucibles, holding specific oxide mixtures, were suspended by a platinum wire (0.5−mm in diameter) in the even zone of the furnace. All samples were pre-melted before equilibration at 1650 °C for 1−3 h, after which the furnace temperature was cooled to 50 °C below the equilibrium temperature for 1 h to promote the crystallization of solid phases. Thereafter, the samples were hold at equilibrium temperature and an that equilibration time of 24 h based on the experience reported by previous authors [19−21] was used to ensure equilibrium had been reached. Ar gas was passed through the furnace during the whole experiment to avoid moisture and other potential contamination sources. The base of the furnace was removed prior to rapidly quenching of the sample directly into ice water. Samples were then dried, crushed and grounded under 300 meshes and mounted in epoxy resin and polished for furthur analysis. X-ray diffraction (XRD), scanning electron microscope (SEM) and energy dispersive X-ray spectroscope (EDX) were used to identify the co-existing phase and analyze the composition of each sample.

3 Results and discussion

3.1 Results of pseudo-melting temperatures

The determined pseudo-melting temperatures of Ti-bearing slags are listed in Table 2, and the average value of T_1, T_2 and T_3 was chosen as the pseudo-melting temperature T.

The pseudo-melting temperatures change gradually with the increase of $w(CaO)/w(SiO_2)$, as shown in Fig. 2. The pseudo-melting temperatures increased from 1319 °C to 1516 °C when $w(CaO)/w(SiO_2)$ increased from 0.90 to 1.64 for 10% TiO_2. It could also be found that the pseudo-melting temperature change with $w(CaO)/w(SiO_2)$ showed two different segments in different areas, namely M6, M23, M8, M9, M24 and M24, M25, M10, M7, M26. The reason for the different gradients may due to the face that the experimental points go across different primary crystal fields when $w(CaO)/w(SiO_2)$ increases. The change is similar when the content of TiO_2 is fixed at other values such as 5%, 15%, 20% or 25%.

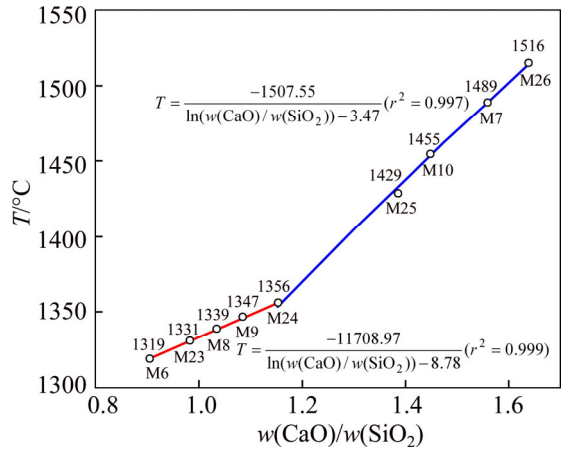

Fig. 2 Relation between pseudo-melting temperature T and $w(CaO)/w(SiO_2)$ for 10% TiO_2

3.2 Construction of liquidus lines

The gradient change in different areas could be explained by the thermodynamic equations, which could be deduced with reference to the isothermal phase diagram in Fig. 3. In the primary phase of B, the point M located on liquidus line represents the equilibrium of solid B with liquid, and from the equilibrium of chemical potential, Eq. (1) could be deduced.

Table 2 Determined pseudo-melting temperatures and calculated temperatures of Ti-bearing slag (°C)

No.	$w(CaO)/w(SiO_2)$	$w(TiO_2)$	T_1/°C	T_2/°C	T_3/°C	T/°C	T_{cal}/°C	ΔT/°C
M1	1.52	4.54	1471	1474	1469	1471	1475	4
M2	1.45	4.65	1449	1447	1445	1447	1452	5
M3	0.94	4.91	1288	1286	1287	1287	1283	−4
M4	1.31	5.21	1418	1415	1420	1418	1408	−10
M5	1.02	5.40	1305	1302	1303	1303	1310	7
M6	0.9	9.13	1318	1323	1317	1319	1319	0
M7	1.56	9.62	1490	1489	1487	1489	1490	1
M8	1.03	9.85	1336	1340	1341	1339	1339	0
M9	1.09	10.59	1348	1346	1347	1347	1347	0
M10	1.45	10.30	1452	1457	1456	1455	1454	−1
M11	1.66	14.23	1519	1510	1513	1514	1519	5
M12	1.45	14.97	1465	1474	1474	1471	1471	0
M13	1.00	15.60	1356	1359	1358	1358	1356	−2
M14	1.58	18.65	1478	1481	1484	1481	1483	2
M15	1.13	18.86	1376	1372	1381	1376	1374	−2
M16	0.90	18.96	1312	1310	1308	1310	1308	−2
M17	1.79	20.74	1529	1531	1532	1531	1530	−1
M18	1.21	27.00	1394	1398	1393	1395	1397	2
M19	0.92	5.33	1279	1280	1280	1280	1275	−5
M20	1.10	5.01	1331	1329	1335	1332	1340	8
M21	1.36	5.18	1430	1431	1432	1431	1425	−6
M22	1.60	4.97	1538	1540	1538	1539	—	—
M23	0.98	10.18	1331	1330	1333	1331	1331	0
M24	1.15	9.67	1353	1355	1359	1356	1354	−2
M25	1.39	10.05	1431	1430	1427	1429	1433	4
M26	1.64	9.58	1515	1516	1518	1516	1515	−1
M27	0.98	15.13	1353	1356	1358	1356	1351	−5
M28	1.21	15.31	1409	1405	1404	1406	1413	7
M29	1.37	14.97	1457	1451	1452	1453	1454	1
M30	1.71	14.43	1532	1535	1536	1534	1530	−4
M31	1.00	21.79	1373	1368	1373	1371	—	—
M32	1.25	20.81	1404	1406	1408	1406	1404	−2
M33	1.52	17.93	1460	1458	1462	1460	1469	9
M34	1.76	18.18	1526	1529	1530	1528	—	—
M35	1.09	28.28	1371	1369	1374	1371	1375	4
M36	1.26	25.64	1406	1407	1408	1407	1407	0
M37	1.52	25.83	1448	1449	1451	1449	1452	3
M38	1.76	22.57	1545	1540	1539	1541	—	—

$T=(T_1+T_2+T_3)/3$; T_{cal} means the calculated temperature; $\Delta T= T_{cal.}-T$.

$$u_{B(L)} = u_{B(S)} \quad (1)$$

The terms $u_{B(L)}$ and $u_{B(S)}$ in Eq. (1) are the chemical potential of liquid B and solid B, respectively. Taking pure solid oxide and pure liquid as standard state, the chemical potentials of solid B and liquid B could be expressed as Eqs. (2) and (3) respectively:

$$u_{B(L)} = u^{\theta}_{B(L)} + RT\ln x_{B(L)} = G^{\theta}_{B(L)} + RT\ln x_{B(L)} \quad (2)$$

$$u_{B(S)} = u^{\theta}_{B(S)} + RT\ln x_{B(S)} = G^{\theta}_{B(S)} + RT\ln x_{B(S)} \quad (3)$$

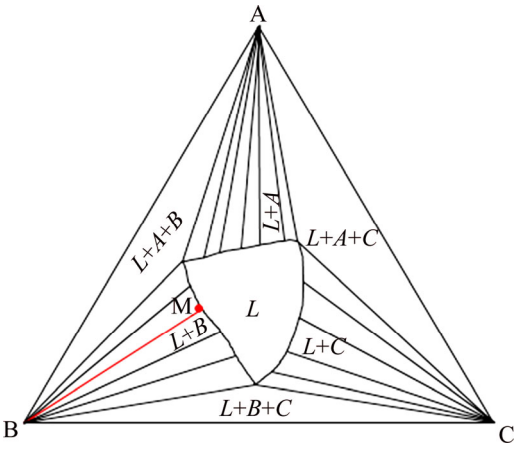

Fig. 3 Schematic of iso-thermal A−B−C phase diagram at temperature of T

where R is the gas constant, T is the iso-thermal temperature, $x_{B(L)}$ and $x_{B(S)}$ are the mass fractions of B in liquid and solid, respectively. The value of $x_{B(L)}$ is 1 when the pure solid oxide is taken as standard state. Combining Eqs. (2) and (3) with Eq. (4) and Gibbs-Helmholtz equation in Eq. (5), the following Eq. (6) could be deduced:

$$\Delta G^{\theta}_{B(fus)}=G^{\theta}_{B(L)}-G^{\theta}_{B(S)} \tag{4}$$

$$\Delta G^{\theta}_{B(fus)}=\Delta H^{\theta}_{B(fus)}(1-\frac{T}{T_m}) \tag{5}$$

$$x_{B(L)}=\exp\left[-\frac{\Delta H^{\theta}_{B(fus)}}{R}\frac{1}{T}+\frac{\Delta H^{\theta}_{B(fus)}}{RT_m})\right] \tag{6}$$

where T_m and $\Delta H^{\theta}_{B(fus)}$ are the melting temperature and molar Gibbs energy of pure solid B respectively. As the value of R, T_m, $\Delta H^{\theta}_{B(fus)}$ are almost constant and the term $x_{B(L)}$ stands for the variables of compositions such as $w(TiO_2)$ and $w(CaO)/w(SiO_2)$, which could be simplified as x. Then Eq. (6) could be simplified as

$$x=\exp(\frac{a}{T}+b) \tag{7}$$

Equation (7) could be further simplified for discussing the relation of T with composition x, as

$$T=\frac{a}{\ln x-b} \tag{8}$$

Equation (8) could be used to fit the relation between the temperature T and composition x in the specific primary crystal field of substance B. $a=-\frac{\Delta H^{\theta}_{B(fus)}}{R}$ and $b=\frac{\Delta H^{\theta}_{B(fus)}}{RT_m}$ a and b could be seen as constant and could be regressive from the melting temperature experimentally measured.

The composition must locate in the same primary crystal field when Eq. (8) is used. However, in the actual fitting process for an unknown phase diagram system, such as the $CaO-SiO_2-5\%MgO-20\%Al_2O_3-TiO_2$ system under research in this work, the experimental points within the same primary crystal field keep uncertain before the regression. Under this circumstance, the following principle is adopted to obtain the optimal fitting: the temperature change with $w(CaO)/w(SiO_2)$ with different contents of TiO_2 is plotted firstly and then the character of gradient is analyzed, after which the points with the same gradient will be regressed together. Taking Fig. 2 as an illustrator, the temperature change with $w(CaO)/w(SiO_2)$ shows two different gradients at 10% TiO_2, then Eq. (8) is applied to each gradient and the fitting effect is good as shown in Fig. 2. The fitting processes at other contents of TiO_2 are done by the same way. Finally, the regressive equations were established for the composition investigated in the present research. The temperatures at the pre-melted composition calculated by the regressive equations agree well with the temperature experimentally determined, which can be found in Table 2. Based on the regressive equations, the liquidus lines of 1300−1500 °C of $CaO-SiO_2-5\%MgO-20\%Al_2O_3-TiO_2$ system are calculated, as shown in Fig. 4. The liquidus temperature increases when $w(CaO)/w(SiO_2)$ increases and the shape of liquidus lines are similar to each other from 1350 °C to 1450 °C.

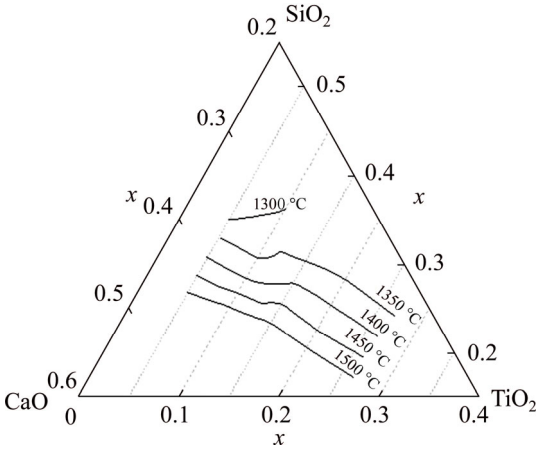

Fig. 4 Calculated 1300−1500 °C liquidus lines for $CaO-SiO_2-5\%MgO-20\%Al_2O_3-TiO_2$ system

3.3 Estimation of equilibria phases

Totally 9 samples, as the soft dots in Fig. 5, were selected for equilibria at 1400 °C to detect the primary crystal in the phase diagram. The SEM micrographs are shown in Fig. 6 to Fig. 10. The equilibria phases were confirmed coupled with the XRD determination. In the following figures, CT stands for $CaO{\cdot}TiO_2$, C_2MS_2 for $2CaO{\cdot}MgO{\cdot}2SiO_2$, C_2AS for $2CaO{\cdot}Al_2O_3{\cdot}SiO_2$ and CMS_2 for $CaO{\cdot}MgO{\cdot}2SiO_2$. Three different two-phase equilibra and one three-phase equilibrium were found in

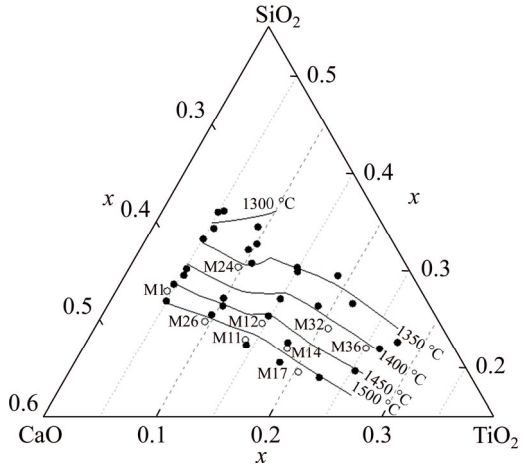

Fig. 5 Equilibria points for CaO−SiO_2−5%MgO−20%Al_2O_3−TiO_2 system at 1400 °C (soft dots)

the samples.

Sample M24 presents as single phase and no crystals were detected in XRD diffraction peaks, which means that M24 was liquid at 1400 °C. On the other hand, this result is consistent with the pseudo-melting temperature determined in Table 2, as the pseudo-melting temperature of M24 being 1356 °C.

Figure 6 shows the typical SEM microphotograph of liquid coexisting with melilite solid solution phase for sample M1. The corresponding XRD result and the EDX results in Table 3 mean that the irregular shaped phase is $(C_2MS_2, C_2AS)_{ss}$ while the light grey phase is liquid.

Figure 7 presents the typical SEM microphotograph and corresponding XRD results of liquid-CT equilibrium (sample M17), in which the white dendritic shape phase is CT while the grey phase is liquid. Figure 8 presents the results of the three-phase equilibrium (sample M11), in which the white phase is CT, while the dark grey phase is $(C_2MS_2, C_2AS)_{ss}$ and the light grey phase is liquid. The liquid-diopside equilibrium is exemplified in Fig. 9, in which the dark grey phase is diopside while the light grey phase is liquid.

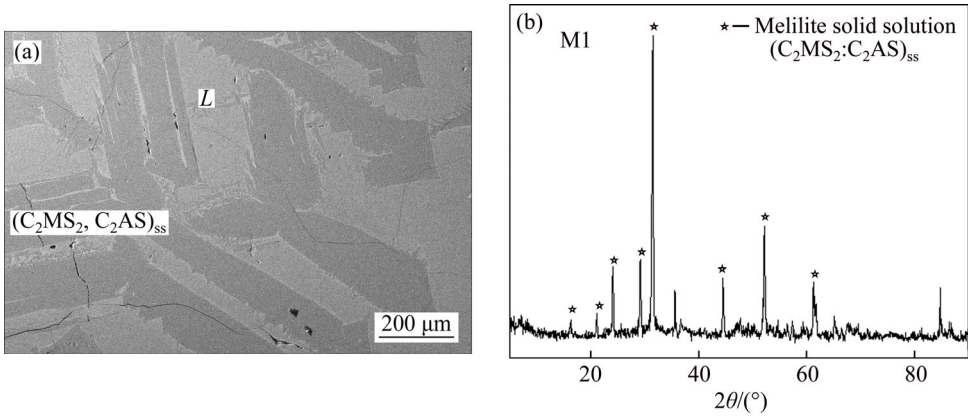

Fig. 6 SEM microphotograph of liquid coexistent with $(C_2MS_2, C_2AS)_{ss}$ at 1400 °C (a) and corresponding XRD result for sample M1 (b)

Table 3 EDX result of sample M1

Phase	Contrast in SEM microphotograph	*x*(O)/%	*x*(Mg)/%	*x*(Al)/%	*x*(Si)/%	*x*(Ca)/%	*x*(Ti)/%
Melilite solid solution	Dark gray	49.47	2.09	14.07	13.40	20.97	—
Liquid	Light gray	55.02	4.03	5.30	13.31	19.67	2.67

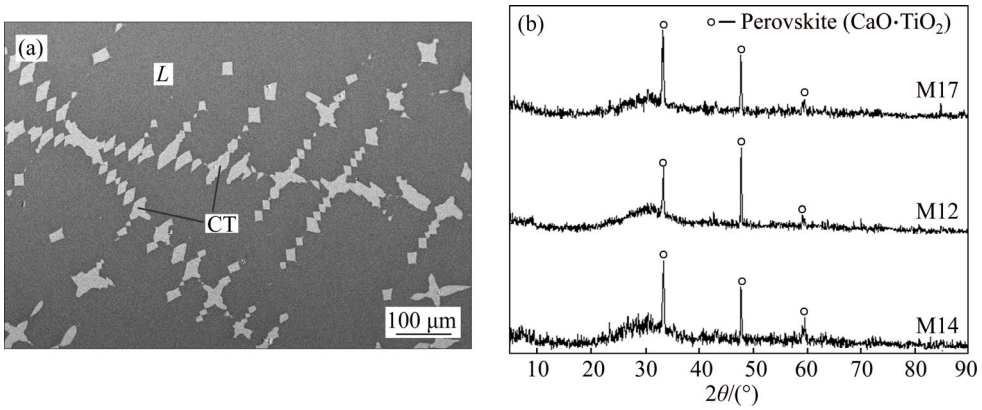

Fig. 7 SEM microphotograph of coexistentence of liquid with CT at 1400 °C for sample M17 (a) and corresponding XRD results for

samples M12, M14 and M17 (b)

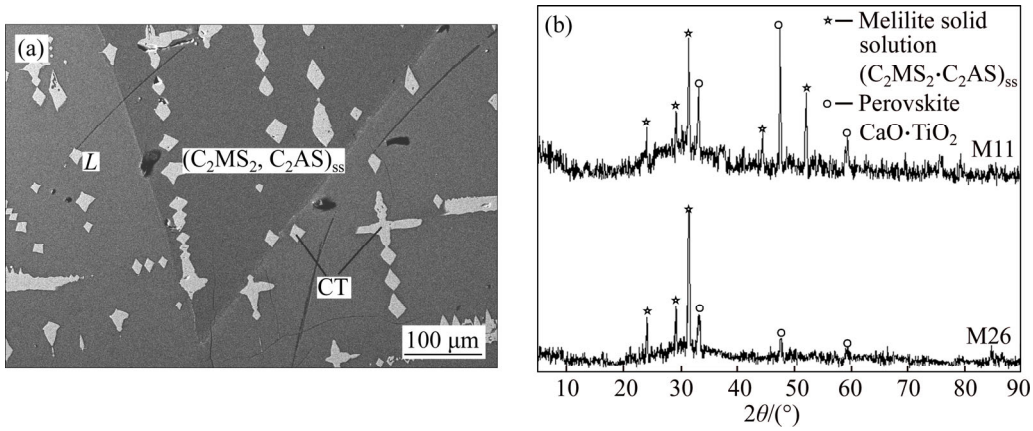

Fig. 8 SEM microphotograph of liquid coexistent with CT and $(C_2MS_2, C_2AS)_{ss}$ at 1400 °C for sample M11 (a) and corresponding XRD results for samples M11 and M26 (b)

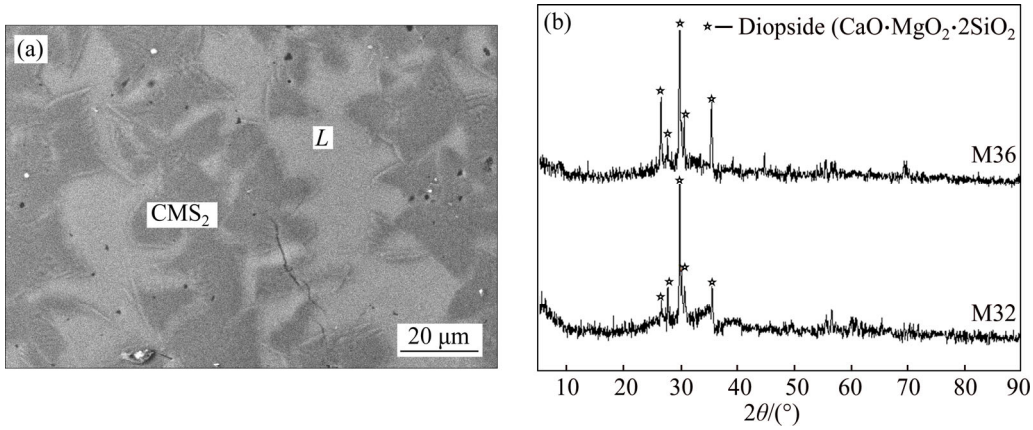

Fig. 9 SEM microphotograph of liquid coexistent with diopside at 1400 °C for sample M36 (a) and corresponding XRD results for samples M32 and M36 (b)

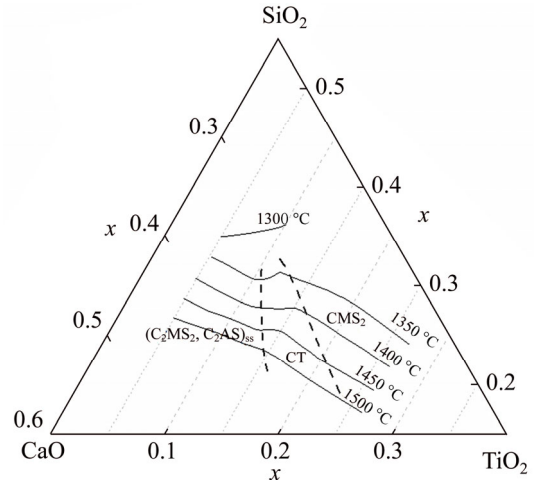

Fig. 10 Brief phase diagram for $CaO{-}SiO_2{-}5\%MgO{-}20\%Al_2O_3{-}TiO_2$ system

3.4 Presentation of phase diagram

Coupling the equilibria phase information with the calculated liquidus lines, a brief phase diagram of $CaO{-}SiO_2{-}5\%MgO{-}20\%Al_2O_3{-}TiO_2$ system with the predicted phase boundary lines (dashed lines) is depicted, as shown in Fig. 10, the high $w(CaO)/w(SiO_2)$ and low TiO_2 content region is dominated by the melilite solid solution phase, while the domination phase changes to perovskite phase when TiO_2 content increases. As a comparison, the diopside phase becomes the domination phase in the higher TiO_2 content and lower $w(CaO)/w(SiO_2)$ area.

4 Conclusions

The pseudo-melting temperatures were determined by the SHTT for the specified content of 5%−25% TiO_2 in the $CaO{-}SiO_2{-}5\%MgO{-}20\%Al_2O_3{-}TiO_2$ phase diagram system, and the 1300 °C−1500 °C liquidus lines were calculated according to thermodynamic equations in the specific primary crystal field. The equilibria phase relationship at 1400 °C was experimentally determined using the quenched technique followed by XRF, XRD, SEM and EDX analysis and the liquid phase, $(C_2MS_2,C_2AS)_{ss}$ solid solution phase, diopside phase (CMS_2) and $CaO{\cdot}TiO_2$ phase were found. Therefore, the

phase diagram was constructed for the specified region of the $CaO-SiO_2-5\%MgO-20\%Al_2O_3-TiO_2$ system.

References

[1] ZHANG Wu, ZHANG Li, ZHANG Ju-hua, FENG Nai-xiang. Crystallization and coarsening kinetics of rutile phase in modified Ti-bearing blast furnace slag [J]. Industrial & Engineering Chemistry Research, 2012, 51(38): 12294−12298.

[2] LIU Xiao-hua, SUI Zhi-tong. Study on leaching Ti-blast furnace slag by pressure [J]. China Nonferrous Met, 2002, 12(6): 1281.

[3] WANG Ming-hua, DU Xing-hong, SUI Zhi-tong. Recovery of titanium from rich titanium blast furnace slag [J]. Multipurpose Util Miner Resour, 2000, 4: 5−7.

[4] BARIN I, SCHULER W. On the kinetics of the chlorination of titanium dioxide in the presence of solid carbon [J]. Metallurgical Transactions B, 1980, 11(2): 199−207.

[5] PENG Yi. Development of technologies for recovering titanium from Pangang BF slag [J]. Titanium Industry Progress, 2005, 22(3): 44−48. (in Chinese)

[6] WANG Yu-ming, LIU Rui-feng, ZHOU Rong-hui, SHAO Bao-shun, WEI Qing-song, YUAN Zhang-fu, XU Chong. Thermodynamics on the reaction of carbochlorination of titania for getting titanium tetrachloride [J]. Computers and Applied Chemistry, 2006, 23(3): 263. (in Chinese)

[7] WANG Xi-dong, MAO Yu-wen, LIU Xiang-ying, ZHU Yuan-kai. Study on crystallization behavior of blast furnace slag containing TiO_2 [J]. J Iron Steel Res, 1990, 3: 1−6.

[8] SUN Yong-qi, LI Jing, WANG Xi-dong, ZHANG Zuo-tai. The effect of P_2O_5 on the crystallization behaviors of Ti-bearing blast furnace slags using single hot thermocouple technique [J]. Metallurgical and Materials Transactions B, 2014, 45(4): 1446−1455.

[9] OLLNO A, ROSS H U. Liquidus-temperature measurements in the lime-titania-alumina-silica system [J]. Canadian Metallurgical Quarterly, 1963, 2(3): 243−258.

[10] OSBORN E F, GEE K H. Phase equilibria at liquidus temperature for a part of the system $CaO-MgO-Al_2O_3-TiO_2-SiO_2$ and their bearing on the effect of titania on the properties of blast furnace slag [J]. Bulletin of the Earth and Mineral Sciences Experiment Station, 1969, (85): 57−80.

[11] ZHAO Bao-jun, EUGENE J A K, HAYES P C. Investigation and application of phase equilibrium of Ti-containing blast furnace slags [C]// The 7th China Steel Conference Proceedings. 2009: 438−442.

[12] VDEH. Slag atlas [M]. Germany: Verlag Stahleisen Gmbh, 1995.

[13] SHI Jun-jie, SUN Li-feng, ZHANG Bo, LIU Xu-qiang, QIU Ji-yu, WANG Zhao-yun, JIANG Mao-fa. Experimental determination of the phase diagram of the $CaO-SiO_2-5pctMgO-10pctAl_2O_3-TiO_2$ system [J]. Metallurgical and Materials Transactions B, 2016, 47(1): 425−433.

[14] SHI Jun-jie, SUN Li-feng, LIU Xu-qiang, QIU Ji-yu, WANG Zhao-yun, JIANG Mao-fa. Experimental determination of the liquidus temperature of $CaO-SiO_2-MgO-10\%Al_2O_3-5\%TiO_2$ system [J]. Journal of Central South University: Science and Technology, 2014, 47(10): 3309−3314. (in Chinese)

[15] KASHIWAYA Y, CICUTTI C E, CRAMB A W, ISHII K. Development of double and single hot thermocouple technique for in situ observation and measurement of mold slag crystallization [J]. ISIJ International, 1998, 38(4): 348−356.

[16] LI Jing, ZHANG Zuo-tai, LIU Li-li, WANG Wan-lin, WANG Xi-dong. Influence of basicity and TiO_2 content on the precipitation behavior of the Ti-bearing blast furnace slags [J]. ISIJ international, 2013, 53(10): 1696−1703.

[17] XIAO Don, WANG Wan-lin, LU Bo-xun. Effects of B_2O_3 and BaO on the crystallization behavior of $CaO-Al_2O_3$−based mold flux for casting high-Al steels [J]. Metallurgical and Materials Transactions B, 2015, 46(2): 873−881.

[18] JAK E, HAYES P C, LEE H G. Improved methodogies for the determination of high temperature phase equilibria [J]. Metals and Materials, 1995, 1(1): 1−8.

[19] GRAN J, WANG Yan-li, DU Si-chen. Experimental determination of the liquidus in the high basicity region in the Al_2O_3 (30mass%)−CaO−MgO−SiO_2 system [J]. CALPHAD, 2011, 35: 249−254.

[20] HENAO H M, KONGOLI F, ITAGAKI K. High temperature phase relations in FeO_x(x=1 and 1.33)-CaO-SiO_2 systems under various oxygen partial pressure [J]. Materials Transactions, 2005, 46(4): 812−819.

[21] KANG Y B, LEE H G. Experimental study of phase equilibria in the MnO−SiO_2− "TiO_2"-"Ti_2O_3" system [J]. ISIJ, 2005, 45(11): 1552−1560.

(Edited by YANG Hua)

Cite this article as: SUN Li-feng, SHI Jun-jie, ZHANG Bo, QIU Ji-yu, WANG Zhao-yun, JIANG Mao-fa. Liquidus and phase equilibria in $CaO-SiO_2-5\%MgO-20\%Al_2O_3-TiO_2$ system [J]. Journal of Central South University, 2017, 24(1): 48−55. DOI: 10.1007/s11771-017-3407-y.